DEVELOPMENTAL BIOLOGY **192,** 274–288 (1997)
ARTICLE NO. DB978765

Hox Group 3 Paralogous Genes Act Synergistically in the Formation of Somitic and Neural Crest-Derived Structures

Nancy R. Manley[1] and Mario R. Capecchi[2]

Howard Hughes Medical Institute, Department of Human Genetics, University of Utah School of Medicine, Salt Lake City, Utah 84112

Hox **genes encode transcription factors that are used to regionalize the mammalian embryo. Analysis of mice carrying targeted mutations in individual and multiple *Hox* genes is beginning to reveal a complex network of interactions among these closely related genes which is responsible for directing the formation of spatially restricted tissues and structures. In this report we present an analysis of the genetic interactions between all members of the third paralogous group, *Hoxa3,* *Hoxb3,* and *Hoxd3.* Previous analysis has shown that although mice homozygous for loss-of-function mutations in either *Hoxa3* or *Hoxd3* have no defects in common, mice mutant for both genes demonstrate that these two genes strongly interact in a dosage-dependent manner. To complete the analysis of this paralogous gene family, mice with a targeted disruption of the *Hoxb3* gene were generated. Homozygous mutants have minor defects at low penetrance in the formation of both the cervical vertebrae and the IXth cranial nerve. Analysis and comparison of all double-mutant combinations demonstrate that all three members of this paralogous group interact synergistically to affect the development of both neuronal and mesenchymal neural crest-derived structures, as well as somitic mesoderm-derived structures. Surprisingly, with respect to the formation of the cervical vertebrae, mice doubly mutant for *Hoxa3* and *Hoxd3* or *Hoxb3* and *Hoxd3* show an indistinguishable defect, loss of the entire atlas. This suggests that the identity of the specific *Hox* genes that are functional in a given region may not be as critical as the total number of *Hox* genes operating in that region.**

INTRODUCTION

Hox genes encode transcription factors belonging to the *Antennapedia* homeodomain class. Man and mouse, and perhaps all mammals, contain 39 *Hox* genes distributed on four linkage groups designated Hox A, B, C, and D. This organization is believed to have arisen early in vertebrate phylogeny by quadruplication of an ancestral complex common to vertebrates and invertebrates (Holland and Garcia-Fernandez, 1996). Based on DNA sequence similarities and the position of the genes on their respective chromosomes, individual members of the four linkage groups have been classified into 13 paralogous families. Members of the same paralogous family share both DNA sequence and gene expression similarities. Mutational analysis in the mouse has demonstrated that these genes are used to regionalize the embryo along its major axes (Chisaka and Capecchi, 1991; Lufkin *et al.,* 1991; Chisaka *et al.,* 1992; LeMouellic *et al.,* 1992; Condie and Capecchi, 1993; Dollé *et al.,* 1993; Gendron-Maguire *et al.,* 1993; Jeannotte *et al.,* 1993; Ramirez-Solis *et al.,* 1993; Rijli *et al.,* 1993; Small and Potter, 1993; Davis and Capecchi, 1994, 1996; Kostic and Capecchi, 1994; Satokata *et al.,* 1995; Suemori *et al.,* 1995; Barrow and Capecchi, 1996; Boulet and Capecchi, 1996; Goddard *et al.,* 1996; Studer *et al.,* 1996; Chen and Capecchi, 1997). Thus, mutations in 3′ *Hox* genes affect the formation of anterior structures, whereas disruption of 5′ genes gives rise to posterior abnormalities. Regionalization of the embryo by *Hox* genes appears to be accomplished by the controlled temporal and spatial activation of these genes such that a 3′ gene is activated prior to and in a more anterior region of the embryo than its 5′ neighbors (Duboule and Dollé, 1989; Graham *et al.,* 1989; Duboule, 1994; Capecchi, 1997). However, *Hox* genes function as highly integrated circuits such

[1] Current address: Institute of Molecular Medicine and Genetics, Department of Pediatrics, Medical College of Georgia, Augusta, Georgia 30912.

[2] To whom correspondence should be addressed. Fax: (801) 585-3425. E-mail: mario.capecchi@genetics.utah.edu.

0012-1606/97 $25.00

that paralogous genes, adjacent genes on the same linkage group, and even nonparalogous genes in separate linkage groups interact positively, negatively, and in parallel with each other to orchestrate the morphological regionalization of the embryo (Condie and Capecchi, 1994; Rancourt *et al.,* 1995; Davis *et al.,* 1995; Horan *et al.,* 1995a, b; Davis and Capecchi, 1996; Favier *et al.,* 1996; Fromental-Ramain *et al.,* 1996; Hérault *et al.,* 1996; Zákány and Duboule, 1996).

In this report we examine the interactions between members of the third paralogous group, *Hoxa3, Hoxb3,* and *Hoxd3*. The phenotypes resulting from targeted disruption of *Hoxa3* and *Hoxd3* have been described (Chisaka and Capecchi, 1991; Condie and Capecchi, 1993). This analysis revealed that disruption of *Hoxa3* resulted primarily in mesenchymal neural crest defects, whereas *Hoxd3* mutant mice showed abnormalities in somitic mesoderm-derived structures. Thus, *Hoxa3* mutant homozygotes are athymic, are aparathyroid, have reduced thyroid tissues, and have malformations in throat cartilages, whereas *Hoxd3* mutant mice show transformations of the cervical vertebrae, C1 and C2, which acquire characteristics associated with more anterior structures.

Although mice mutant for either *Hoxa3* or *Hoxd3* alone did not show overlapping defects, mice mutant for both *Hoxa3* and *Hoxd3* demonstrated that these genes strongly interact. In the double mutants, the *Hoxd3* mutation strongly exacerbated the *Hoxa3* defects, and conversely the *Hoxd3*-associated mutant defects were strongly enhanced by the *Hoxa3* mutation (Condie and Capecchi, 1994).

In order to extend the analysis of the role of the group 3 paralogs during embryonic development, we have disrupted the remaining member of this group, *Hoxb3*. Unlike those of its paralogs, *Hoxb3* homozygous mutants survive to adulthood and are fertile. Analysis of the skeletal and central nervous systems shows minor and low-penetrance defects in the cervical vertebrae and IXth cranial nerve. We also examined the phenotypes of all three double mutant classes. The double mutant analysis revealed strong synergistic interactions between all three members of this paralogous group in both somitic mesoderm and mesenchymal and neuronal neural crest-derived structures. Surprisingly, with respect to defects in the formation of the cervical vertebrae, *Hoxa3/Hoxd3* and *Hoxb3/Hoxd3* double mutants are indistinguishable, suggesting that it is the number of *Hox* genes operating within a region which appears to be critical rather than their specific identity. Further, the severity of the abnormality is proportional to the number of mutant *Hox* gene alleles carried by the mutant mouse. The importance of quantitative interactions among *Hox* genes is further illustrated by comparison of mice individually heterozygous for group 3 paralogous gene mutations, with mice heterozygous for mutations in all three genes. Mice individually heterozygous for *Hoxa3, Hoxb3,* or *Hoxd3* are viable, are fertile, and show no abnormalities or only very minor, low-penetrance defects in the formation of the cervical vertebrae. However, most mice heterozygous for all three genes die prior to weaning.

MATERIALS AND METHODS

Targeting Vector Construction

Genomic DNA containing the *Hoxb3* locus was isolated from a genomic library prepared from DNA isolated from the ES cell line CC1.2 and probed with a 51-bp oligonucleotide located at the 3′ end of the *Hoxb3* homeobox (Graham *et al.,* 1988; Condie and Capecchi, 1993). Sequences containing the homeobox were deleted by partial digestion with *Eag*I and replaced by the insertion of the MC1neopA cassette, which confers neomycin resistance (Thomas and Capecchi, 1987). The resulting deletion removed 226 bp, beginning 5 bases 5′ of the homeobox and ending 40 bp 3′ of the homeobox. The final targeting vector contained 10 kb of genomic DNA including the mutated allele, flanked by the *TK1* and *TK2* herpes simplex virus *thymidine kinase* genes (Fig. 1A).

Generation of Hoxb3 Mutant Mice

The *Hoxb3* targeting vector was linearized and electroporated into J1 ES cells (Lee *et al.,* 1992). Electroporated cells were cultured using positive/negative selection in G418 and FIAU (Mansour *et al.,* 1988). Clones containing a correctly targeted allele of *Hoxb3* were identified by Southern blot analysis (Fig. 1). Fidelity of the homologous recombination events were confirmed by Southern blot analysis with four restriction enzymes, using 5′ and 3′ flanking probes and a probe specific for the *neo*^{r} gene (Fig. 1 and data not shown). Positive cell lines were injected into C57BL/6J (BL/6) blastocysts. Male chimeras were backcrossed to BL/6 females, and offspring derived from ES cells were identified by coat color and genotyped by Southern blot analysis or PCR (Fig. 1 and below).

Genotype Analysis for Hoxb3

Mice and embryos were genotyped by either Southern blot or PCR analysis of tail or yolk sac DNA. For Southern blot analysis, genomic DNA was digested with *Eco*RI and probed with the 3′ flanking probe (probe 1, Fig. 1A). The wild-type allele is within an approximately 28-kb fragment, while the mutant allele yields a 5.7-kb fragment due to the insertion of the *neo*^{r} gene (Figs. 1C and 1D).

PCR analysis was performed in 20-μl reactions amplified for 34 cycles with 10 s at 94°C, 20 s at 65°C, and 30 s at 72°C. Three *Hoxb3*-specific PCR primers and one *neo*^{r} gene-specific primer were used to genotype animals and to confirm the structure of the deletion/insertion in the mutant allele. The *Hoxb3*-specific primers were primer 1, located just 5′ of the homeobox, 5′ACAAGAGCCCCCCGGGGTC3′ (nucleotides 546–564; Sham *et al.,* 1992); primer 2, located just inside the 5′ end of the homeobox, 5′CAAGCGGGCGCGCACGGCGTAC3′ (nucleotides 574–595; Sham *et al.,* 1992); and primer 3, from the antisense strand, located 3′ of the intended deletion, 5′AACCCTTAAGAGGGGGCTGGTAG3′ (nucleotides 953–931; Sham *et al.,* 1992). Two *neo*^{r} gene-specific primers were used. Primer 4 was located on the sense strand at the 3′ end of the MC1neopA cassette, 5′TCTATCGCCTTCTTGACGAGTTC3′. Primer 5 was located on the antisense strand at the 5′ end of MC1neopA, 5′CGTGTTCGAATTCGCCAATGACAAGAC3′ (Figs. 1E and 1F). For the wild-type allele, primers 1 and 3 gave a 407-bp product, and primers 2 and 3 gave a 379-bp product. For the mutant allele, primers 3 and 4 gave a 240-bp product and primers 1 and 5 gave a 220-bp product. Primer 2 does not make a

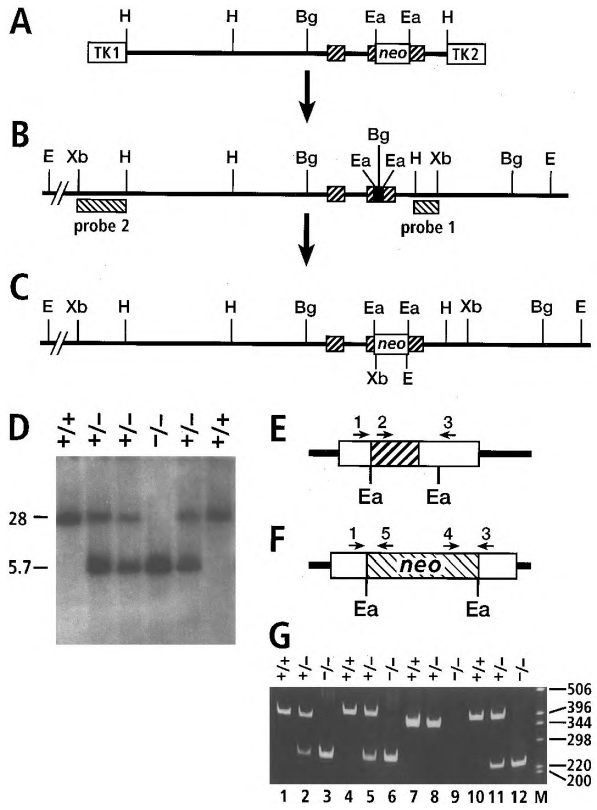

FIG. 1. Gene targeting at the *Hoxb3* locus. (A–D) Horizontal thin lines represent noncoding genomic DNA. Boxes with heavy diagonal lines represent exons, with the homeobox shown in black. (A) Map of the *Hoxb3* targeting vector. The vector contains 10 kb of genomic DNA from the *Hoxb3* locus. A 226-bp *Eag*I fragment encoding the entire *Hoxb3* homeodomain was deleted and replaced with a *neo*^{r} gene. The genomic DNA is flanked by TK genes to provide negative selectable markers. (B) Map of the wild-type *Hoxb3* locus. Probes flanking the DNA sequences present in the targeting vector are indicated. (C) Map of the correctly targeted locus. After homologous recombination between the targeting vector and the *Hoxb3* locus, the resulting mutant allele contains the *neo*^{r} gene in place of the homeobox. Digestion of the wild-type and targeted loci with restriction enzymes yields the following fragment sizes when probed with probe 1, the 3′ flanking probe: *Eco*RI, wt 28 kb, mutant 5.7 kb; *Xba*I, wt 12 kb, mutant 3 kb; and *Bgl*II, wt 4.3 kb, mutant 7.9 kb. H, *Hin*dIII; Bg, *Bgl*II; Ea, *Eag*I; E, *Eco*RI; Xb, *Xba*I; TK, thymidine kinase gene. (D) Southern blot analysis of 3-week-old offspring from a *Hoxb3* heterozygous intercross. Tail DNA was digested with *Eco*RI and probed with probe 1. +/+, +/−, and −/−, wild type, heterozygous, and homozygous mutant DNA samples, respectively. Fragment sizes are indicated in kilobases. (E–G) PCR strategy for genotyping and confirming the genomic structure of the mutation. The wild-type structure of exon 2 is shown in E, and the expected exon 2 structure for the mutant allele is shown in F. All primer pairs used the same 3′ primer, primer 3. Primer 1 was present in both wild-type and mutant alleles, primer 2 was contained within the expected deletion, and primers 4 and 5 were specific to the *neo*^{r} gene. (G) PCR analysis of wild-type and homozygous mutant tail DNAs. Sizes of marker bands (M) are shown in base pairs. Genotypes of DNA samples used are indicated above each lane. Primer combinations used in PCR are lanes 1–3, primers 2, 3, and 4; lanes 4–6, primers 1, 3, and 4; lanes 7–9, primers 2, 3, and 5; and lanes 10–12, primers 1, 3, and 5. No product corresponding to the mutant allele is present in lanes 8 and 9, because primer 2 is deleted in the mutant allele.

product with either neo-specific primer, because it is located within the deletion. PCR products were analyzed using polyacrylamide gel electrophoresis (Fig. 1G).

Generation of Single and Double Mutants

Mice identified as heterozygous for the *Hoxb3* mutation were intercrossed to expand the colony and generate *Hoxb3* homozygous mutants. Litters were collected for analysis during gestation, on the day of birth, or at weaning to assess viability. Embryonic age was estimated by considering noon of the day of a vaginal plug to be E0.5. As *Hoxb3* homozygous mutants survive and are fertile, litters were also produced from homozygous mutant animals.

Mouse colonies for the two double mutants, *Hoxa3/Hoxb3* and *Hoxb3/Hoxd3,* were generated by crossing either *Hoxb3* heterozygous or homozygous mutants with *Hoxa3* or *Hoxd3* heterozygotes, respectively. The mutant alleles of the *Hoxa3* and *Hoxd3* genes have been described previously (Chisaka and Capecchi, 1991; Condie and Capecchi, 1993). Mice generated in the colonies were genotyped for *Hoxa3* and *Hoxd3* by Southern blot or PCR analysis as previously described (Chisaka and Capecchi, 1991; Condie and Capecchi, 1993; Manley and Capecchi, 1995). Double mutants were generated by intercrossing double-heterozygous animals within each colony. Animals which were homozygous for the *Hoxb3* mutation and heterozygous for either of the other paralogs were also used as parents in crosses to generate double mutants. All colonies used for this analysis were maintained on a mixed C57BL6 × 129Sv background.

Skeletal Analysis

Skeletons of newborn mice were stained with alcian blue 8GX and alizarin red as described (Mansour *et al.,* 1993). Adult skeletons were stained only with alizarin red (Davis and Capecchi, 1994).

Immunohistochemistry

Detection of neurofilament protein was performed using the 2H3 anti-155-kDa neurofilament monoclonal antibody obtained from the Developmental Studies Hybridoma Bank (Dodd *et al.,* 1988). Whole-mount immunohistochemistry was performed essentially as described (Davis *et al.,* 1991). Briefly, embryos were fixed in methanol:DMSO (4:1) overnight, treated with hydrogen peroxide to inactivate endogenous peroxidases, rehydrated, and incubated overnight in the 2H3 antibody at a 1:4 dilution in PBSTMD (PBS, 0.5% Triton X-100, 2% skim milk, 1% DMSO). Embryos were washed in PBSTMD and incubated overnight with an HRP-conjugated secondary antibody at 1:100 in PBSTMD. After washing, color reactions were performed in diaminobenzidine and hydrogen peroxide. Embryos were cleared in 1:2 benzyl benzoate:benzyl alcohol for analysis and photographed using a Leitz dissecting microscope.

TABLE 1
Genotypes of Offspring from *Hoxb3* Heterozygous Intercrosses

	+/+	+/−	−/−	Total
P0	24 (30)	62 (59)	33 (30)	119
4 weeks	32 (27)	53 (54)	23 (27)	108

Note. +/+, +/−, and −/− are wild type, heterozygote, and homozygous mutant, respectively. Numbers are listed as observed (expected). Litters of newborn animals (P0) were collected as close to the time of birth as possible. All genotype classes are represented in the expected Mendelian ratios.

RESULTS

Targeted Disruption of the Hoxb3 Gene

A mutant allele of the *Hoxb3* gene was made by homologous recombination, in which a 226-bp *Eag*I fragment encoding the entire *Hoxb3* homeodomain was deleted and replaced with the MC1neopA cassette (Fig. 1A; Thomas and Capecchi, 1987). The resulting deletion should create a loss-of-function allele for DNA binding. The targeting vector, containing 10 kb of genomic DNA from the *Hoxb3* locus, was linearized and introduced into J1 ES cells by electroporation. Cell lines in which a homologous recombination event had occurred were enriched by positive/negative selection and screened by Southern blot analysis (Mansour *et al.,* 1988). In 16 of 144 cell lines analyzed, a correctly targeted allele of *Hoxb3* was observed. These cell lines were further tested by Southern transfer analysis using a total of four restriction enzymes and three probes, 3′ and 5′ flanking probes and a *neo*^{r} probe, to ensure that no rearrangements or duplications had occurred at the targeted locus (data not shown).

The targeted cell line 2h-4 was injected into BL/6 blastocysts and surgically transferred into the uterus of a foster mother to allow the embryos to come to term. Male chimeras were bred to BL/6 females, and a mouse strain carrying the *Hoxb3* mutant allele was established. Animals heterozygous for the *Hoxb3* mutant allele were viable and fertile and had no observed mutant phenotype.

Hoxb3 Homozygous Mutants Are Viable and Fertile

Mice heterozygous for the *Hoxb3* mutation were intercrossed and the genotypes of the offspring determined. Litters were either genotyped at weaning (3–4 weeks) or collected and genotyped immediately after birth (Fig. 1D, Table 1). No significant reduction was seen in the expected number of homozygous mutant animals at either age, indicating that these mutant animals are viable. This result is in strong contrast to that seen with mutations in the paralogous genes *Hoxa3* and *Hoxd3* (Chisaka and Capecchi, 1991; Condie and Capecchi, 1993), in which mutation of the *Hoxa3* gene causes neonatal lethality, and only ~15% of *Hoxd3* mutants survive to weaning. *Hoxb3*$^{-/-}$ adults are fertile and show no obvious outward defects. PCR analysis confirmed that the DNA binding domain of the *Hoxb3* gene had been deleted in the mutant allele (Fig. 1G and Materials and Methods).

Hoxb3 Mutants Have a Minor Defect in the Cervical Vertebrae

Mice that are mutant for either *Hoxa3* or *Hoxd3* have nonoverlapping mutant phenotypes (Chisaka and Capecchi, 1991; Condie and Capecchi, 1993). Mutation of either of these genes causes defects in the formation of the skeleton; however, the affected structures are of separate embryological origin. *Hoxa3* mutants show malformations and reductions in the neural crest-derived cartilages and skeletal elements of the throat, while *Hoxd3* mutants display transformations and deletions in the first and second cervical vertebrae, which are derived from somitic mesoderm. Skeletal preparations from *Hoxb3* intercross newborn litters and adult animals were examined to determine if mutation of the *Hoxb3* gene resulted in defects in any of these or other skeletal structures.

Eighteen newborn and nine adult *Hoxb3*$^{-/-}$ animals were examined for skeletal defects in whole-mount preparations. Mice were scored for the presence of any abnormalities in the skull, vertebral column, throat cartilages, and bones. Structures which were known to be affected in either the *Hoxa3* or the *Hoxd3* mutants were examined carefully for overlapping phenotypes in the *Hoxb3* mutant. No defects were seen in the neural crest-derived cartilages and bones of the throat, nor were any transformations or deletions of cervical vertebrae observed in the *Hoxb3* mutants (Figs. 2B and 3B). Therefore, neither the *Hoxa3* nor the *Hoxd3* single-mutant skeletal phenotype was seen in the *Hoxb3* mutants. However, a minor defect in the formation of the atlas and axis was seen in the *Hoxb3*$^{-/-}$ newborn skeletons. At a low frequency (2 of 18 examined) the anterior arch of the atlas and the dens of the axis were joined by an ossified bridge not normally present in wild-type mice (Fig. 2B). This particular defect was not seen in the *Hoxd3*$^{-/-}$ skeletons, although *Hoxd3*$^{-/-}$ mutants do have defects in the anterior arch of the atlas and in the dens (Fig. 2D; Condie and Capecchi, 1993). Therefore, even though *Hoxb3* and *Hoxd3* do not have overlapping phenotypes, the *Hoxb3* mutation does weakly affect the development of some of the same axial skeletal structures as *Hoxd3*.

The Hoxb3 Mutation Exacerbates both Hoxa3 and Hoxd3 Single Mutant Skeletal Phenotypes

Double mutants between *Hoxa3* and *Hoxd3* revealed that these genes interact synergistically to affect the development of both somitic mesoderm and neural crest-derived skeletal structures (Condie and Capecchi, 1994). To determine whether mutations in *Hoxb3* would also enhance the

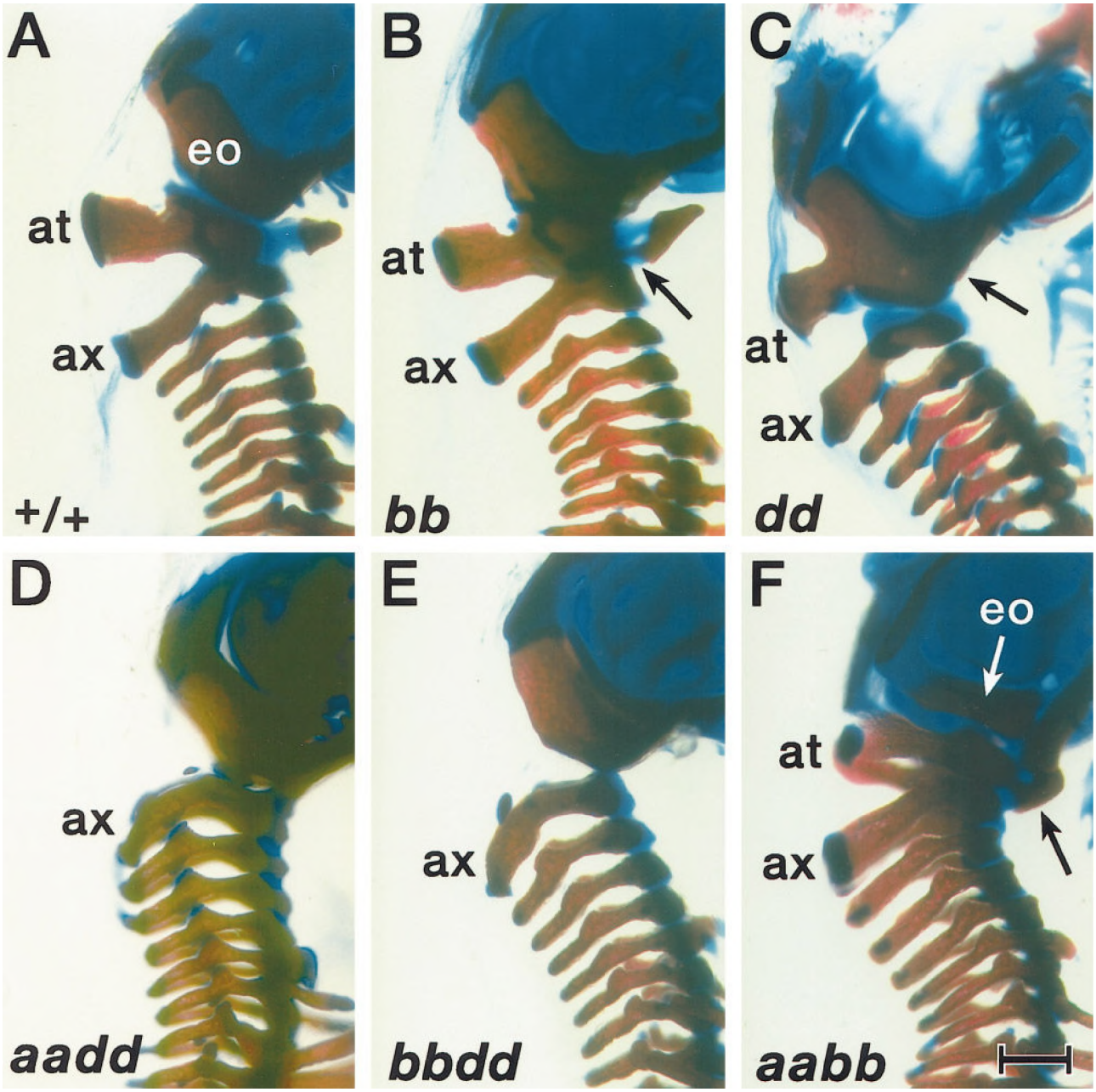

FIG. 2. *Hoxb3* and *Hoxa3* mutations both enhance the *Hoxd3* skeletal phenotype. Lateral views of the cervical region in cleared skeleton preparations of single- and double-mutant newborn mice; dorsal is to the left, anterior is to the top. Genotypes are in the lower left corners, with lowercase letters representing the mutant allele, for example, *bb*, $Hoxb3^{-/-}$; *aadd*, $Hoxa3^{-/-}/Hoxd3^{-/-}$. (A) Wild-type (+/+) control, with atlas (at), axis (ax), and exoccipital (eo) bones indicated. (B) Similar view of a *Hoxb3* mutant; the arrow shows the ossified fusion between the anterior arch of the atlas and the dens of the axis. (C) A *Hoxd3* homozygous mutant, showing the characteristic fusions between the atlas and the bones of the skull. The arrow indicates the deletion of the anterior arch of the atlas and fusion of the atlas to the basioccipital bone at the base of the skull. (D) $Hoxa3^{-/-}/Hoxd3^{-/-}$ double mutant, in which the atlas is deleted and the axis appears transformed toward a more posterior phenotype ($Hoxd3^{-/-}$ and $Hoxa3^{-/-}/Hoxd3^{-/-}$ phenotypes are described in Condie and Capecchi, 1993, 1994). (E) The $Hoxb3^{-/-}/Hoxd3^{-/-}$ double mutant is nearly indistiguishable from the double mutant skeleton in D, with a similar deletion of the atlas and transformation of the axis. (F) The $Hoxa3^{-/-}/Hoxb3^{-/-}$ skeleton also has defects in the atlas and exoccipital bones. The exoccipital bones are markedly reduced in size (eo, white arrow). The anterior arch of the atlas is fused to the basioccipital bone and to the dens (black arrow), and the neural arches are reduced in size. Scale bar, 1 mm.

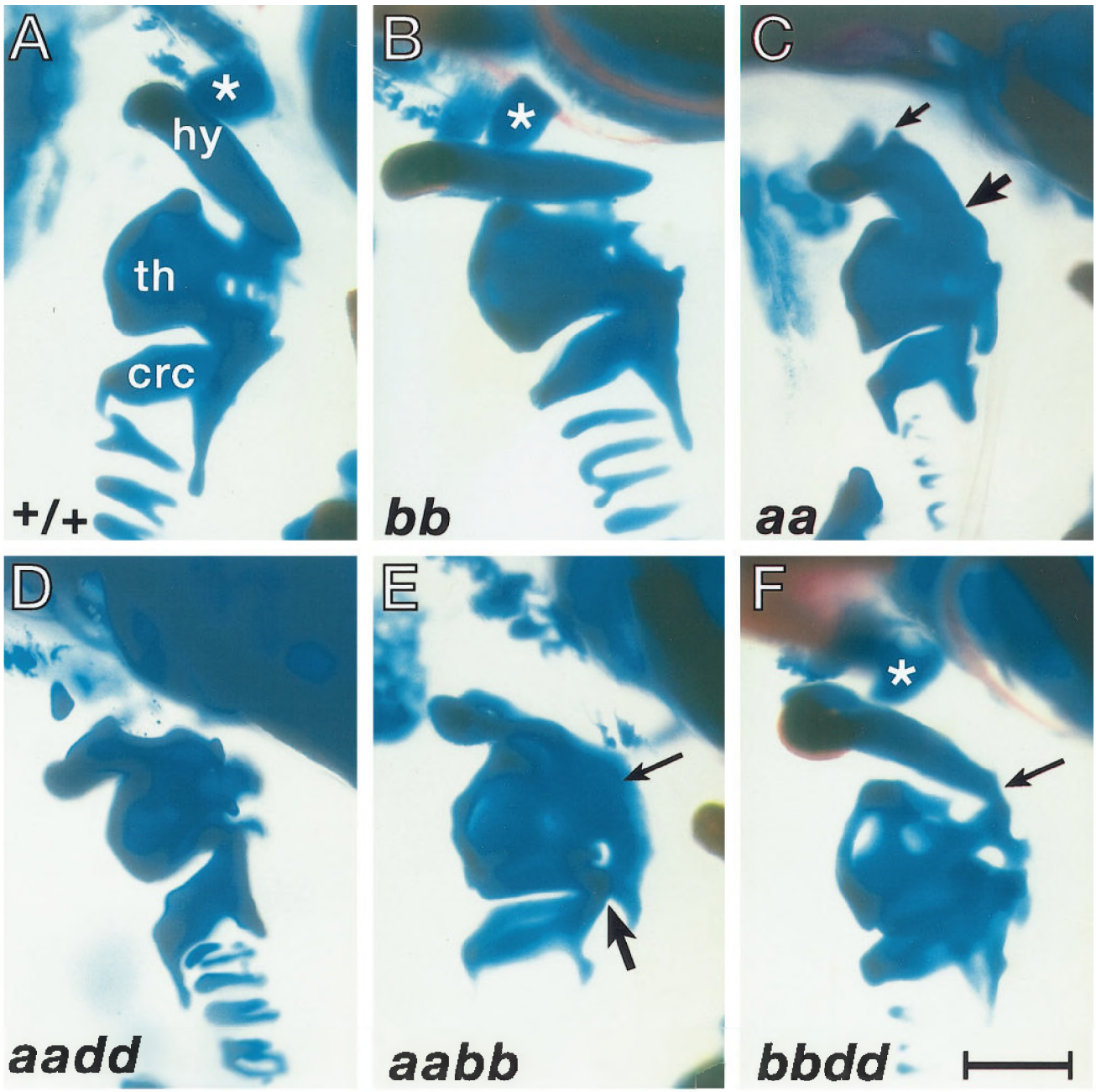

FIG. 3. Mutation of *Hoxb3* enhances the *Hoxa3* mutant phenotype in the throat cartilages. Lateral views of the throat cartilages in cleared skeletal preparations of single- and double-mutant newborn mice; dorsal is to the right, anterior is to the top. Genotypes are in the lower left corners, with lowercase letters representing the mutant allele, for example, *bb, Hoxb3*$^{-/-}$*; aadd, Hoxa3*$^{-/-}$*/Hoxd3*$^{-/-}$. (A) Wild-type (+/+) control, with the greater horn of the hyoid bone (hy), thyroid (thy), and cricoid (crc) cartilages marked. The lesser horn of the hyoid is indicated (star). (B) *Hoxb3*$^{-/-}$ animals have no defects in these structures. (C) *Hoxa3* mutant, showing characteristic reductions and fusions in the hyoid bones and thyroid and cricoid cartilages (described in Chisaka and Capecchi, 1991). The lesser horn of the hyoid is almost completely deleted, and is fused to the greater horn (small arrow). The greater horn is also reduced, malformed, and fused to the thyroid cartilage (large arrow). (D) The *Hoxa3*$^{-/-}$*/Hoxd3*$^{-/-}$ double mutant has more severe defects, primarily in the hyoid bones (described in Condie and Capecchi, 1994). (E) The *Hoxa3*$^{-/-}$*/Hoxb3*$^{-/-}$ double mutant also shows severe reductions in the hyoid, including complete deletion of the lesser horn. The thyroid cartilage is poorly formed, with the dorsal aspect showing an amorphous mass of cartilage (small arrow). The cricoid cartilage is also fused to the thyroid cartilage (large arrow). (F) The *Hoxb3*$^{-/-}$*/Hoxd3*$^{-/-}$ double mutant shows minor defects, with the greater horn of the hyoid fused to the thyroid cartilage (arrow). The lesser horn is unaffected (star). The thyroid and cricoid cartilages are also malformed. Scale bar, 0.5 mm.

TABLE 2
Genotypes of Newborns from Double Heterozygous Intercrosses

	a3, b3 observed (expected)	b3, d3 observed (expected)
+/+,+/+	5 (7.5)	6 (6)
+/−,+/+	15 (15)	16 (12)
+/+,+/−	17 (15)	13 (12)
+/−,+/−	36 (30)	20 (24)
−/−,+/+	2 (7.5)	7 (6)
+/+,−/−	10 (7.5)	7 (6)
+/−,−/−	17 (15)	9 (12)
−/−,+/−	14 (15)	11 (12)
−/−,−/−	3 (7.5)	9 (6)
Total	119	98

Note. +/+, +/−, and −/− are wild type, heterozygous, and homozygous mutant, respectively. Litters of newborn animals were collected as close to the time of birth as possible. Newborn animals listed include pups recovered both dead and alive. Reduced numbers of newborns recovered in classes which are homozygous mutant for *Hoxa3* were presumably lost due to cannibalization, as these animals die soon after birth (Chisaka and Capecchi, 1991). All remaining genotype classes are represented within the expected Mendelian ratios.

phenotypes of the *Hoxa3* and *Hoxd3* mutants, colonies of both *Hoxa3/Hoxb3* and *Hoxb3/Hoxd3* compound heterozygotes were established. Both *Hoxa3/Hoxb3* and *Hoxb3/Hoxd3* compound heterozygotes were outwardly normal and fertile, and mice within these colonies were intercrossed to produce double mutants.

Both $Hoxa3^{+/-}/Hoxb3^{-/-}$ and $Hoxb3^{-/-}/Hoxd3^{+/-}$ animals survived to adulthood and were fertile. *Hoxa3/Hoxb3* and *Hoxb3/Hoxd3* double mutants survive to birth (Table 2). However, both double mutant classes died either at P0 or before weaning. *Hoxa3/Hoxb3* mutants died within hours of birth, as did *Hoxa3* single mutants. Fifty percent of *Hoxb3/Hoxd3* mutants died at birth, with the remainder dying within the first postnatal week. As *Hoxd3* single mutants usually died within the first week, with some surviving to adulthood, the increase in observed death of *Hoxb3/Hoxd3* double mutants at birth and the 0% viability at weaning represent an exacerbation of this *Hoxd3* phenotype.

Both *Hoxa3/Hoxb3* and *Hoxb3/Hoxd3* double mutants were examined for the ability of the *Hoxb3* mutation to exacerbate the *Hoxa3* and *Hoxd3* single-mutant skeletal phenotypes (Table 3). These results were also compared to the phenotype of the *Hoxa3/Hoxd3* double mutant described previously. The phenotype of the *Hoxb3/Hoxd3* double mutant was much more severe than that seen in either single mutant and was indistinguishable from that seen in the *Hoxa3/Hoxd3* double mutant (Fig. 2). The entire atlas was deleted, with only small cartilage remnants remaining. The axis was also affected, with the neural arch frequently remodeled to resemble the appearance of the more posterior cervical vertebrae C3–C5. The change in the shape of C2 is also in common with *Hoxa3/Hoxd3* double mutants. These results suggest that *Hoxb3* and *Hoxa3* play equivalent roles in combination with *Hoxd3* to mediate the formation of the atlas and axis.

Hoxa3/Hoxb3 double mutants also had defects in the development of the cervical vertebrae and skull (Fig. 2F), even though neither single mutant had a significant defect in the formation of the axial skeleton. Some of these defects are similar to those seen in the *Hoxd3* single mutants, such as fusion of the anterior arch of the atlas to the basioccipital bone and reduction of the neural arches of the atlas and axis (compare Fig. 2C to 2F). However, some defects were different from those seen in *Hoxd3* single mutants. In particular, all of the *Hoxa3/Hoxb3* double mutants examined showed a reduction in the size of the exoccipital bones. These results indicate that the *Hoxd3* gene alone is not sufficient for proper development of the skull and cervical vertebrae, and that all three genes play a role in the normal development of these somitically derived structures.

Examination of the mesenchymal neural crest-derived throat cartilages and bones uncovered similar gene interactions. These structures are affected by mutation of the *Hoxa3* gene, but are normal in both the *Hoxb3* and the *Hoxd3* single mutants (Figs. 3A–3C and Table 3). The *Hoxa3/Hoxb3* double mutant showed an enhancement of the mutant phenotype, which was most prevalent in anterior structures, in particular the greater horn of the hyoid bone, which was almost entirely missing in the *Hoxa3/Hoxb3* double mutant (Fig. 3E). The thyroid cartilage was also poorly formed, appearing as a mass of cartilage with poorly defined structure. The cricoid cartilage was smaller and occasionally fused to the thyroid cartilage. Again, the increased severity in this mutant phenotype was very similar to that seen in the *Hoxa3/Hoxd3* double mutants (compare Fig. 3E to 3D).

The *Hoxb3/Hoxd3* double mutant also showed defects in the throat cartilages and bones (Fig. 3F), which are not affected by the mutation of either individual gene (Fig. 3B and Condie and Capecchi, 1994). These defects were milder than those seen in the *Hoxa3* mutant and affected only a subset of the structures affected by mutation of the *Hoxa3* gene (Fig. 3C). The lesser horn of the hyoid was unaffected, but the greater horn was sometimes fused to the thyroid cartilage, and the thyroid cartilage itself was malformed. These defects were also less penetrant than the axial skeleton defects seen in the *Hoxa3/Hoxb3* double mutants, occurring in about 20% of *Hoxb3/Hoxd3* double mutants examined (see Table 3). Thus, although *Hoxb3* and *Hoxd3* do play a role in the formation of these neural crest-derived structures, expression of the *Hoxa3* gene alone is usually sufficient to specify their normal development.

Enhancement of the Hoxa3 and Hoxd3 Phenotypes by Hoxb3 Is Dosage Sensitive

Analysis of various combinations of *Hoxa3* and *Hoxd3* mutant alleles showed that the interaction of these two

TABLE 3
Double Mutant Newborn Skeletal Defects Summary

	bb	BbDd	bbDd	dd[a]	Bbdd	bbdd	AaBb	Aabb	aa[a]	aaBb	aabb
Axial skeleton											
Basioccipital enlarged posterior edge		77 (10)	100 (9)	67 (4)	89 (8)	100 (9)		8 (1)			60 (3)
Exoccipital											
Reduced										58 (7)	100 (5)
Enlarged				17 (1)	89 (8)	89 (8)					
Supraoccipital remodeled						11 (1)				17 (2)	100 (5)
Anterior arch of atlas											
Fused to dens/split in two	11 (2)	46 (6)	22 (2)				15 (2)	38 (5)		33 (4)	
Deleted/fused to basiocciptal		15 (2)	67 (6)	100 (6)	100 (9)	100 (9)	8 (1)	8 (1)			60 (3)
Atlas											
Fused to exoccipital (lm or foramina)				50 (3)	100 (9)					41 (5)	80 (4)
Foramina deleted		30 (4)	22 (2)	50 (3)	22 (2)		8 (1)			17 (2)	60 (3)
Neural arch reduced/remodeled		100 (13)	100 (3)	100 (6)	100 (9)			23 (3)		67 (8)	100 (5)
Atlas deleted						100 (9)					
Axis											
Dens deleted			11 (1)	100 (6)	100 (9)	100 (9)					
Atlas foramina/anterior arch on axis			22 (2)	50 (3)	100 (9)	100 (9)					
Neural arch broadened (C2 to C1)		46 (6)	67 (6)	17 (1)	44 (4)	11 (1)				17 (2)	60 (3)
Neural arch remodeled		38 (5)	22 (2)		33 (3)	78 (7)		8 (1)			
Atlas/axis neural arches fused			11 (1)		44 (4)						
Throat cartilages (NC)											
Hyoid lesser horn											
Reduced/remodeled									87 (7)	58 (7)	
Deleted									13 (1)	41 (5)	100 (5)
Hyoid greater horn											
Reduced								8 (1)	100 (8)	100 (12)	100 (5)
Fused to thyroid cartilage						22 (2)	8 (1)	23 (3)	100 (8)	100 (12)	100 (5)
Thyroid cartilage reduced/remodeled						22 (2)	8 (1)	23 (3)	100 (8)	100 (12)	100 (5)
Cricoid cartilage reduced/remodeled								38 (5)	100 (8)	100 (12)	100 (5)
Total No. analyzed	18	13	9	6	9	9	13	13	8	12	5

Note. Frequencies of defects are shown as percentages, with the actual number of animals showing the defect in parentheses. The total number of each genotype analyzed is shown at the bottom of each column. If no number is listed, the percentage is zero. Genotypes are represented with capital letters for wild type and small letters for the mutant allele, i.e., Bbdd is $Hoxb3^{+/-}/Hoxd3^{-/-}$.

[a] *Hoxa3* and *Hoxd3* single and the *Hoxa3/Hoxd3* double mutant phenotypes have been previously described (Chisaka and Capecchi, 1991; Condie and Capecchi, 1994, 1995).

genes in the development of these structures is dosage sensitive (Condie and Capecchi, 1994). To determine if the effects of the *Hoxb3* mutation on the *Hoxa3* and *Hoxd3* mutant phenotypes were also dosage dependent, skeletons of mice with intermediate genotypes were examined and compared to the single- and double-mutant phenotypes. Both the $Hoxd3^{-/-}$ axial skeleton phenotype and the $Hoxa3^{-/-}$ throat cartilage defects were enhanced by the removal of a single copy of *Hoxb3* (Fig. 4 and Table 3). These phenotypes were intermediate between the single- and the double-mutant phenotypes, indicating quantitative interactions between these genes.

For *Hoxb3* and *Hoxd3,* removal of one functional copy of *Hoxb3* in the $Hoxd3^{-/-}$ mutant background resulted in the partial loss of the atlas (Fig. 4C). This result is very similar to the defects observed in $Hoxa3^{+/-}/Hoxd3^{-/-}$ mutant mice (Condie and Capecchi, 1994). In addition, increased penetrance was seen for the presence of an anterior arch and/or lateral foramina on the axis, structures normally present on the atlas. The latter indicates that the transformation of C2 toward C1 identity was more complete in $Hoxb3^{+/-}/Hoxd3^{-/-}$ than in $Hoxd3^{-/-}$ mutant mice.

In the case of *Hoxa3* and *Hoxb3,* intermediate phenotypes were seen in both the axial skeleton and the throat cartilages with the progressive removal of copies of these two genes (Figs. 4E–4H and Table 3). Removal of any three alleles of these two genes (i.e., $Hoxa3^{+/-}/Hoxb3^{-/-}$ or $Hoxa3^{-/-}/Hoxb3^{+/-}$) produced an increase in penetrance of the $Hoxb3^{-/-}$ axial skeleton phenotype to about 35%, compared to 11% in the $Hoxb3^{-/-}$ animals. New-

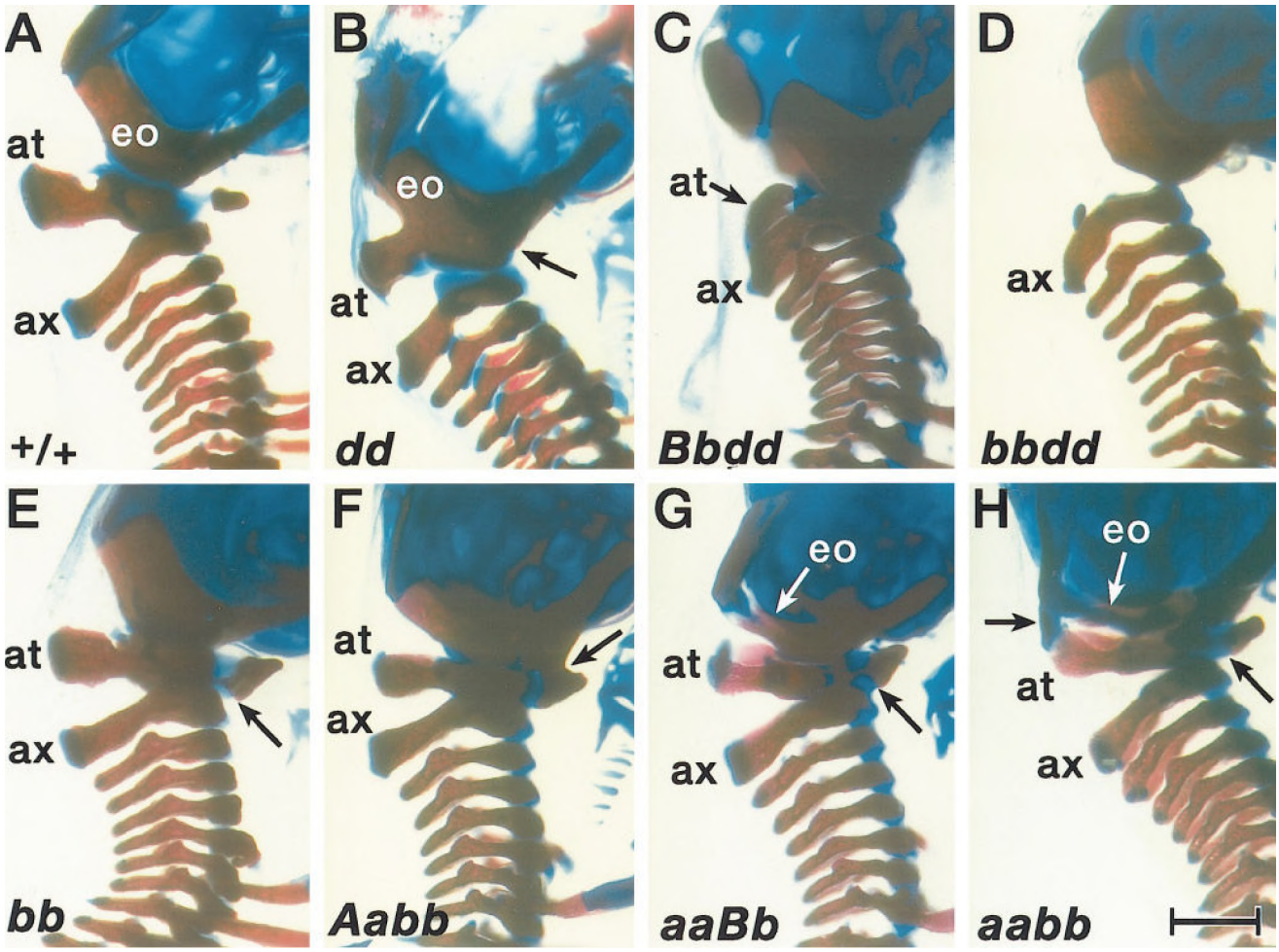

FIG. 4. Enhancement of the *Hoxa3* and *Hoxd3* phenotypes by *Hoxb3* is dosage-sensitive. Lateral views of the cervical region in cleared skeleton preparations of newborn mice; dorsal is to the left, anterior is to the top. Genotypes are in the lower left corners, with uppercase letters representing wild-type alleles and lowercase letters representing the mutant allele, for example, *dd, Hoxd3*$^{-/-}$*; Bbdd, Hoxb3*$^{+/-}$*/Hoxd3*$^{-/-}$. (A) Wild-type (+/+) control, with atlas (at), axis (ax), and exoccipital (eo) bones indicated. (B) *Hoxd3*$^{-/-}$ mutant; the arrow indicates the deletion of the anterior arch of the atlas and fusion of the atlas to the basioccipital bone at the base of the skull. (C) Removal of one copy of *Hoxb3* results in a more severe reduction of the anterior arch of the atlas (arrow), while the *Hoxb3*$^{-/-}$*/Hoxd3*$^{-/-}$ double mutant shows a complete deletion of the atlas (D). (E) A *Hoxb3*$^{-/-}$ mutant, showing an ossified fusion of the anterior arch of the atlas and the dens of the axis (arrow). (F) Removal of one copy of *Hoxa3* results in additional fusion of the anterior arch to the base of the skull (arrow) and a reduction in the atlas neural arch (at). (G) Removal of one copy of *Hoxb3* in a *Hoxa3* mutant also results in reductions in the atlas (at) and exoccipital bones (eo, white arrow). These mice also have a fusion of the atlas anterior arch to the dens (black arrow), a phenotype that is seen in *Hoxb3*$^{-/-}$ mice. (H) The *Hoxa3*$^{-/-}$*/Hoxb3*$^{-/-}$ double mutants have further reductions in the atlas and exoccipitals. This example also shows a dorsal fusion of the atlas neural arch to the skull (short black arrow) and the atlas anterior arch fused to the axis (long black arrow). Scale bar, 1 mm.

borns with these genotypes also displayed defects in the formation of the atlas and, to a lesser extent, the axis (Figs. 4F and 4G), defects which were not seen in either single mutant. These axial skeleton defects included a subset of those seen in *Hoxd3*$^{-/-}$ animals, but were less penetrant and less severe. In *Hoxa3/Hoxb3* double mutants the severity and penetrance of these defects increased, but never reached the severity of defects seen in the absence of *Hoxd3*.

In the throat cartilages, the removal of one copy of *Hoxb3* in the *Hoxa3* mutants also resulted in an increase in the severity of the deformities seen. This was most dramatically seen as a progressively more complete deletion of the lesser horn of the hyoid bone and reduction in size of the greater

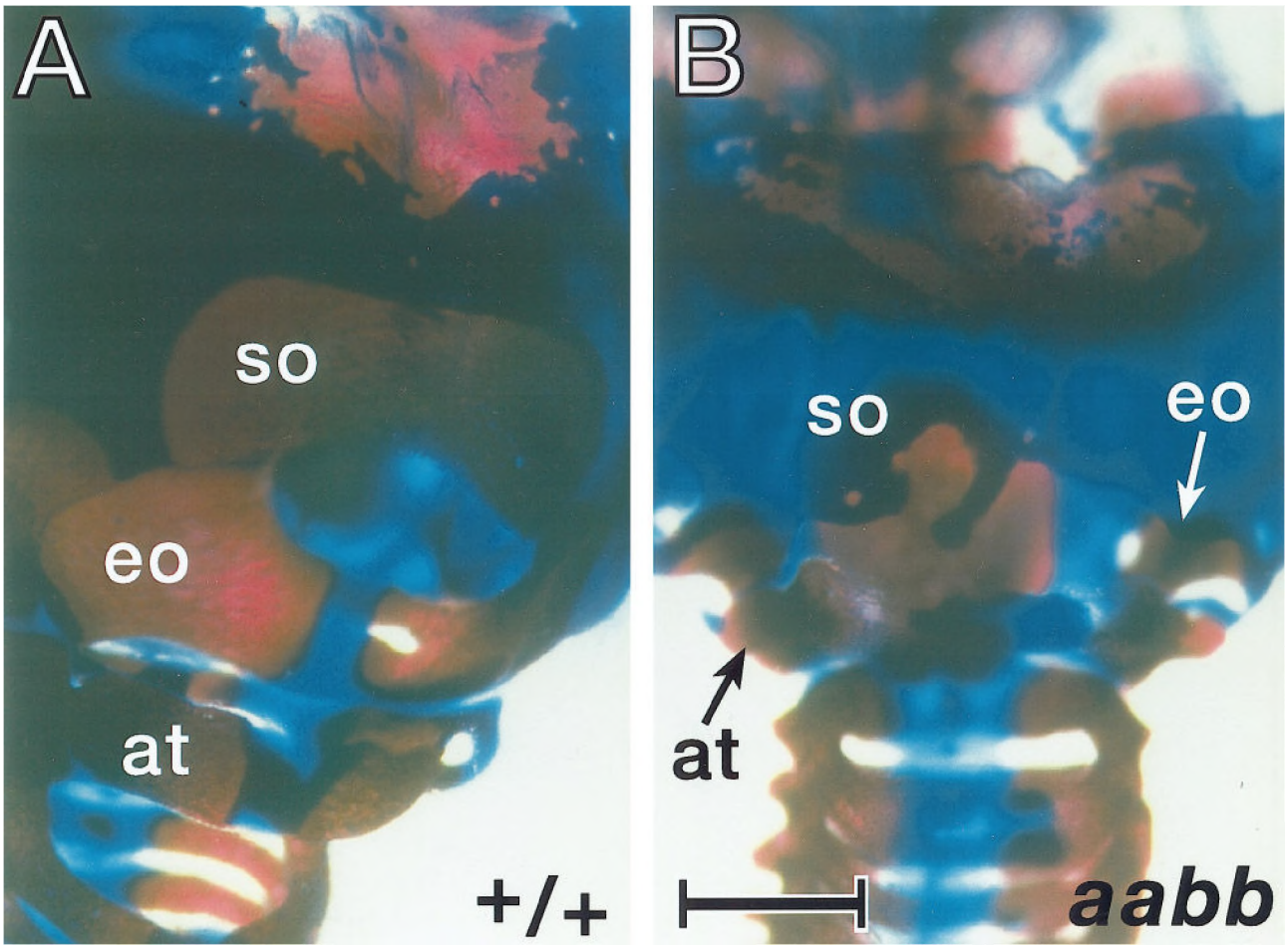

FIG. 5. The supraoccipital bone is deformed in double mutants. Dorsal view of the base of the skull and upper cervical region of newborn skeletons; anterior is up. (A) Wild-type (+/+) control. The supraoccipital bone (so) is well formed and completely ossified. The exoccipitals (eo) and atlas neural arches (at) are also indicated. (B) In *Hoxa3*$^{-/-}$/*Hoxb3*$^{-/-}$ double mutants (*aabb*), the supraoccipital is severely malformed and not ossified. The exoccipitals and atlas neural arches are very reduced (see also Figs. 2 and 4). Scale bar, 1 mm.

horn (Table 3). In addition, removal of one copy of *Hoxa3* in the *Hoxb3*$^{-/-}$ background resulted in some defects in the hyoid bone and throat cartilages, none of which were seen in the *Hoxb3* mutants alone (Table 3).

Double Mutants Have a Novel Skeletal Defect

In addition to increased severity of single-mutant phenotypes, all three double mutants were found to have defects in the formation of the supraoccipital bone of the skull (Fig. 5). The penetrance of this defect ranged from 10% in *Hoxb3/Hoxd3* double mutants to 20% in *Hoxa3/Hoxd3* double mutants to 100% in the *Hoxa3/Hoxb3* double mutants (Table 3). In addition, this defect (2 of 12 examined) was seen at low penetrance in *Hoxa3*$^{-/-}$/*Hoxb3*$^{+/-}$ newborns. The supraoccipital bone appeared normal in all other genotype classes. The appearance in the double mutants of defects in a structure not affected by any of the single mutants suggests that the development of this structure represents a more highly redundant function of these genes, particularly when the *Hoxa3* and *Hoxb3* genes are involved. The low penetrance of defects in double mutant classes including the *Hoxd3* mutation, and the 100% penetrance of the defect in *Hoxa3/Hoxb3* double mutants, indicate that *Hoxd3* has a relatively minor function in the development of the supraoccipital bone.

The Hoxa3 and Hoxb3 Single Mutants Have Defects in the Formation of the IXth Cranial Nerve

Although *Hoxa3*$^{-/-}$ newborns were previously examined histologically for the presence of the cranial ganglia, an embryonic analysis of the development of the cranial nerves and ganglia was not performed. Neurofilament staining of

TABLE 4
Summary of Embryonic Neurofilament Analysis of Group 3 Single and Double Mutants

	+/+	aa	bb	dd[a]	aabb	aadd	bbdd
IXth cranial ganglion unconnected to hindbrain[b]		25 (3)[c]	5 (1)		11 (1)	17 (1)	
IX/X fusion[b]		50 (6)	9 (2)		66 (6)	33 (2)	42 (3)
Unconnected/fused[d]		8 (1)			22 (2)	33 (2)	
Total No. affected	0 (0)	83 (10)	14 (3)	0 (0)	100 (9)	83 (5)	42 (3)
Total No. unaffected	100 (6)	17 (2)	86 (19)	100 (4)	0 (0)	17 (1)	57 (4)
Total No. analyzed	6	112	22	4	9	6	7

[a] *Hoxd3* single-mutant phenotype was also previously analyzed and reported to be normal (Condie and Capecchi, 1993).
[b] Includes both unilateral and bilateral phenotypes.
[c] Percentage of total (number observed).
[d] Embryos which had an unconnected IXth cranial ganglion on one side and a IX/X fusion on the other side.

Hoxa3$^{-/-}$ embryos revealed defects in the formation of the IXth cranial nerve in 10 of 12 mutant homozygous embryos examined (Table 4). These defects fell into two classes. In 25% of embryos examined there was an apparent deletion of the proximal portion of the IXth cranial ganglion, with a remaining patch of neurofilament-positive cells in the normal location of the distal portion of the ganglion (Figs. 6B and 6E). These embryos appeared to have at least some part of the IXth cranial ganglion, but it was not connected to the hindbrain. This phenotype may represent the deletion of neural crest-derived cells that contribute to the formation of the superior ganglion, with the remaining neurofilament-positive cells representing the inferior petrosal ganglion, which is thought to be placode derived.

The second class of mutant phenotype seen in the *Hoxa3* mutant embryos was a fusion of the IXth and Xth cranial

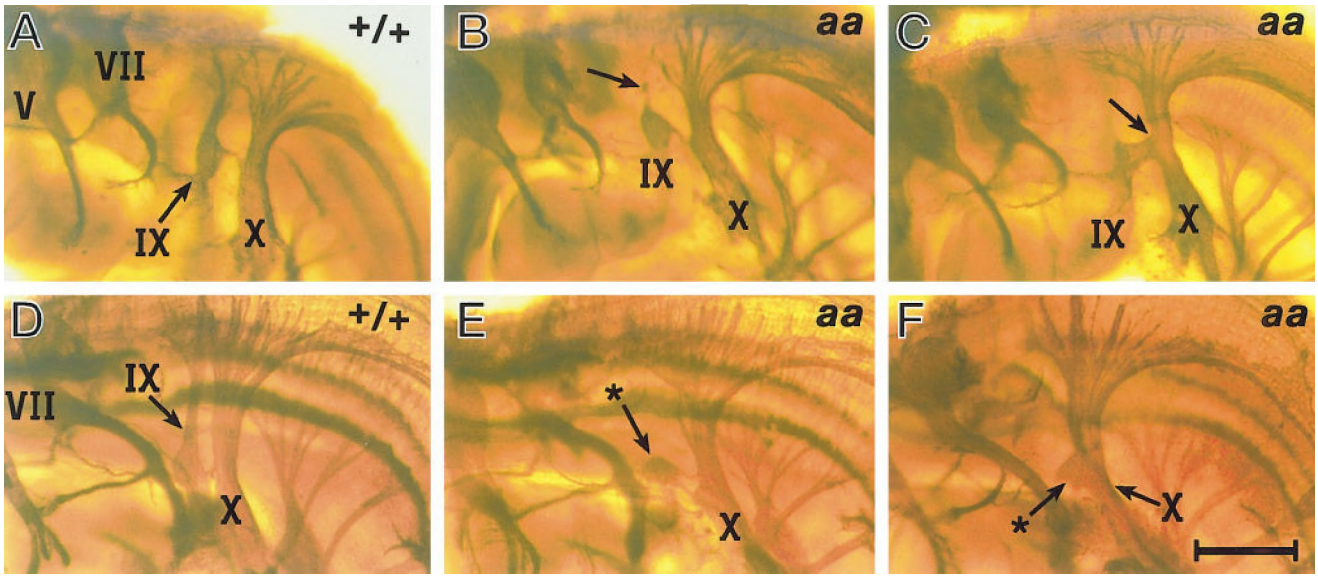

FIG. 6. Development of the cranial nerves is defective in *Hoxa3* mutants. Lateral views of cleared embryos stained in whole mount with the 2H3 anti-neurofilament antibody; dorsal is up, anterior is to the left. Genotypes are shown as +/+, wild type; and *aa*, *Hoxa3*$^{-/-}$. All visible cranial ganglia are identified in A and D, by roman numerals (V, VII, IX, and X). (A–C) E10.5 embryos. (A) In control embryos, all cranial ganglia are present and have readily visible connections to the hindbrain. (B) A *Hoxa3* mutant with a class I IXth cranial ganglion mutant phenotype, in which there is a patch of neurofilament-positive cells in the correct location for the IXth cranial ganglion, but with no apparent connection to the hindbrain (arrow). (C) A *Hoxa3* mutant with a fusion of the IXth and Xth ganglia (arrow). (D–F) E11.5 embryos. (D) At this stage the cranial nerves are well developed, and the IXth and Xth cranial ganglia are close together, but still clearly separated. (E) The IXth cranial ganglion in this *Hoxa3* mutant appears as only a small patch (star). (F) *Hoxa3* mutant appears to have a nearly complete fusion of the IXth and Xth cranial ganglia; what may be the remnants of the IXth cranial ganglion are indicated (star). Scale bar, 0.5 mm.

ganglia, occurring in 50% of *Hoxa3* mutants examined (Figs. 6C and 6F). It is possible that this phenotype may result from the same deletion of proximal structures described above. The IXth and Xth cranial ganglia normally become closely associated as embryonic development proceeds, and at birth they are difficult to distinguish. The fusion of these two ganglia seen in the *Hoxa3* mutants was quite different from the normal close association of these ganglia since the IXth nerve appeared to have no independent connection to the hindbrain. This fusion was most clearly evident at E10.5, a stage when G IX and G X are normally well separated (Figs. 6A and 6C). At E11.5, this defect could be sometimes construed as a deletion of the IX ganglion (Fig. 6F). However, as no cases of complete deletion of the IXth ganglion were ever seen at E10.5, it is most likely that these represent extreme cases of fusion, rather than total deletion.

All of the $Hoxa3^{-/-}$ embryos with the deletion of the proximal portion of the IXth ganglion had a bilateral defect. The IX/X fusion defects were seen both bilaterally and unilaterally. In addition, one embryo showed a "mixed" phenotype, with a IX/X fusion on one side and a deletion of the proximal portion of the IXth ganglion on the other.

Examination of the cranial nerves in $Hoxb3^{-/-}$ embryos showed that both classes of cranial ganglion phenotype were also present in these mutants, but at a much lower penetrance. Only 14% (3/22) showed defects; however, the nature of the defects seen in these embryos was the same as that seen in the $Hoxa3^{-/-}$ embryos (Table 4). Two of these embryos had defects that were unilateral, and one embryo had a bilateral IX/X fusion. The *Hoxb3* mutants therefore have defects in structures of two separate embryological origins, somitic mesoderm and neuronal neural crest, but these defects are present at a low penetrance. The cranial nerves in $Hoxd3^{-/-}$ embryos were previously analyzed by this method and shown to be normal (Condie and Capecchi, 1993). That result was confirmed in this analysis (Table 4).

Double-Mutant Analysis of Cranial Nerve Development

The above analysis showed that two of the genes in this paralogous group have defects in the formation of the IXth cranial ganglion, albeit with varying penetrance. To determine if *Hoxd3* plays a role in development of the cranial ganglia, double mutants of all three classes were analyzed by neurofilament staining. Because the percentage of $Hoxa3^{-/-}$ animals showing the cranial nerve defects was already quite high, and the defects were probably the result of a deletion of structures (the neural crest-derived cells of the ganglion), it was difficult to assess an increase in the severity of penetrance of the *Hoxa3* phenotype in the *Hoxa3/Hoxb3* and *Hoxa3/Hoxd3* double mutants. The relative percentages of the two classes of mutant phenotypes did not significantly change, nor did the percentage of bilateral vs unilateral defects increase (Table 4). However, in the *Hoxb3/Hoxd3* double mutants, an increase from 14 to 42% was seen in the penetrance of the IXth cranial ganglion defects over that observed in the *Hoxb3* single mutant. This increase in penetrance shows that *Hoxd3* does play a role in cranial nerve development, even though the *Hoxd3* single mutant does not show a defect in these structures. In over 50% of cases, however, two functional copies of the *Hoxa3* gene alone were apparently capable of directing correct development of these structures. These results are similar to those seen in the mesenchymal neural crest-derived throat cartilages.

DISCUSSION

Initial genetic analysis of group 3 paralogous *Hox* gene family members showed that disruption of *Hoxa3* resulted in defects in tissues derived from the neural crest (Chisaka and Capecchi, 1991), whereas mutations in *Hoxd3* showed defects in somitic mesoderm-derived tissues (Condie and Capecchi, 1993). These results suggested that although these two paralogous genes were operating in the same region of the embryo, they functioned in tissues of separate embryonic origins. However, analysis of mice mutant for both genes revealed a more complex picture. Although no overlap in function was evident in mice homozygous for disruptions in either individual gene, in the double mutant it was clear that the presence of the *Hoxd3* mutant alleles exacerbated the *Hoxa3* defects, and conversely the *Hoxa3* mutation enhanced the *Hoxd3* mutant phenotype (Condie and Capecchi, 1994). Further, the degree of exacerbation was proportional to the total number of disrupted alleles carried by the mutant mice. These results suggest that both *Hoxa3* and *Hoxd3* are functional in neural crest and somitic mesoderm-derived tissues but that the role of *Hoxa3* in forming the atlas and axis only becomes apparent in the absence of *Hoxd3* function. Similarly, the role of *Hoxd3* in the development of neural crest-derived tissues was only evident in *Hoxa3* mutant homozygotes.

The data described in this report extend this concept by showing that not only do these paralogous genes operate in multiple tissues in the same region of the embryo, but also often appear to be performing equivalent functions within these tissues. This is particularly evident in the formation of the cervical vertebrae, where *Hoxa3/Hoxd3* and *Hoxb3/Hoxd3* double mutants have indistinguishable defects, the deletion of the entire atlas. Similar function is also apparent in the formation of the IXth nerve, in which all three double mutants show the same defect, the loss of the neural crest-derived components of the IXth nerve, but differ only in the penetrance of this defect.

The observation that the contributions of *Hoxa3* and *Hoxb3* in forming the atlas and axis appear to be equivalent in *Hoxd3* mutant homozygotes suggests that the identity of the *Hox* genes operating in the developing tissue is not as critical a factor as the number of *Hox* genes functioning within this tissue. In further support of this concept, mice that are heterozygous for the *Hoxa3* and *Hoxb3* mutations and homozygous for the *Hoxd3* mutation (i.e., $Hoxa3^{+/-}$/

Hoxb3$^{+/-}$/*Hoxd3*$^{-/-}$ mice) show the same C1, C2 defects observed in *Hoxa3/Hoxd3* or *Hoxb3/Hoxd3* double mutants (unpublished data). Thus, the perspective changes from a qualitative one to a quantitative one. A molecular interpretation of this phenomenon suggests that individual *Hox* genes may not be individually responsible for implementing a unique developmental program, but rather that multiple *Hox* genes function together to mediate a program by controlling common target genes through common *cis* elements and that for proper development it is the stoichiometry of *Hox* genes operating within a developing tissue that is critical.

In the absence of *Hoxd3,* the roles of *Hoxa3* and *Hoxb3* in forming the cervical vertebrae C1 and C2 appear to be equivalent. Nevertheless, *Hoxd3* is more important than its paralogs in mediating the formation of these vertebrae. Similarly, *Hoxa3* predominates over *Hoxb3* and *Hoxd3* in directing the formation of neural crest-derived structures. Such differences could be explained either by the production of more *Hoxd3* or *Hoxa3* protein in somitic mesoderm or neural crest cells, respectively, or by *Hoxd3* and *Hoxa3* proteins having higher affinities for common vertebral or neural crest tissue target gene *cis* elements, respectively.

The deletion of the atlas in *Hoxa3/Hoxd3* and *Hoxb3/Hoxd3* double mutants would not have been predicted from the analysis of mice individually homozygous for mutations in *Hoxa3, Hoxb3,* or *Hoxd3. Hoxa3* mutant homozygotes show no apparent defects in the formation of the atlas, *Hoxb3* mutant homozygotes show mild and low penetrant defects in the formation of the anterior arch of the atlas, and *Hoxd3* mutant mice have changes in the shape of the atlas so that it resembles the shape of its neighboring anterior skull components, the ex- and basioccipital bones. The deletion of the atlas in the double mutants suggests a role for these *Hox* genes in the establishment, the proliferation, and/or the maintenance of the prechondrogenic anlage used to form the atlas.

Comparison of the results reported here with those of Horan *et al.* (1995a, b) is instructive. These authors examined the effects of combining mutations in multiple members of the group 4 paralogous genes. Rather than deletions of cervical vertebrae, the second and more posterior cervical vertebrae acquired shape characteristics associated with the first cervical vertebra, the atlas. Combining increasing numbers of group 4 mutant alleles progressively increased the extent and number of cervical vertebrae demonstrating this transformation. Preliminary analysis of mice mutant for all three group 3 paralogous genes suggests that increasing the number of mutant alleles of these genes progressively extends the deletion of cervical vertebrae beyond C1 (unpublished data). The contrasting results obtained by combining either group 3 or group 4 mutant alleles suggest that while both sets of genes are required for the formation of cervical vertebrae, they function at different times during development. The group 3 genes would be required early in development and their absence results in early failure to form the cervical vertebrae, whereas the group 4 genes would function later in development, causing changes in the identity of vertebral structures which have already been specified to form. Both of these mutant phenotypes are consistent with *Hox* genes functioning to influence cell proliferation but at different times during development of these structures. Consistent with this hypothesis, *Hox* group 3 genes are activated prior to *Hox* group 4 genes (Duboule and Dollé, 1989; Graham *et al.,* 1989).

The suggested roles for group 3 and group 4 paralogous genes in forming the cervical vertebrae are in accord with models proposed for more posterior genes in mediating the formation of the limbs. Loss-of-function mutations affecting limb development are also most readily interpreted in terms of changes in cell proliferation (Dollé *et al.,* 1993; Potter and Small, 1993; Davis and Capecchi, 1994, 1996). In addition, the analysis of mice with multiple *Hox* gene mutations indicates that multiple *Hox* genes are used quantitatively to control the growth and patterning of the limbs, and that the identity of the *Hox* gene that is mutated may be less critical than the number of *Hox* genes operating in a given limb zone (Davis *et al.,* 1995; Davis and Capecchi, 1996; Favier *et al.,* 1996; Fromental-Ramain *et al.,* 1996; Hérault *et al.,* 1996; Zákány and Duboule, 1996). Finally, since in *Hoxa11/Hoxd11* double mutants only a vestige of the radius and ulna is formed, whereas in *Hoxa11/Hoxd12* double mutants the length of these long bones is reduced to approximately one-half of their normal length, the suggestion again arises that these *Hox* genes are functioning in limb development during at least two separate phases, during the specification of the prechondrogenic condensations and during the outgrowth of the long bones themselves (Davis and Capecchi, 1996). During the patterning of the vertebral column and limbs, *Hox* genes could readily be modulating the activity of very similar sets of target genes.

Analysis of the role of group 3 paralogous genes in the development of the cranial nerves has revealed a previously unreported phenotype for the *Hoxa3* mutation in the development of the IXth cranial nerve. The results indicate that *Hoxa3* functions in both neuronal and mesenchymal neural crest. This mutant phenotype represents an apparent overlap with defects reported for *Hoxa2* mutants, which also show a deletion of the proximal portion of the IXth cranial nerve. *Hoxa2* mutants display a deletion of the lesser horn and a reduction of the greater horn of the hyoid bone, which are also reduced or deleted in *Hoxa3* mutants. However, previous reports have shown that expression of the *Hoxa2* gene was not changed in *Hoxa3* mutant embryos, nor is *Hoxa3* expression altered in *Hoxa2* mutants (Gendron-Maguire *et al.,* 1993; Rijli *et al.,* 1993; Manley and Capecchi, 1995). Therefore, these overlapping mutant phenotypes appear to represent common functions for these two neighboring genes. The *Hoxb3* mutation also does not appear to alter expression of the neighboring *Hoxb2* and *Hoxb4* genes. Consistent with this observation, *Hoxb3* mutant defects do not overlap with *Hoxb2* and *Hoxb4* mutant phenotypes. This is in contrast to the *Hoxb2* mutation which critically

alters both *Hoxb1* and *Hoxb4* expression (Barrow and Capecchi, 1996).

The cause of early neonatal death observed in *Hoxa3* mutant homozygotes in all of the group 3 double mutant combinations, and even in the triple heterozygous mice, has not been determined. However, the proportion of mice that die shortly after birth correlates with the proportion of mice showing bilateral defects in the formation of the IXth nerve. The IXth cranial nerve, or glossopharyngeal nerve, innervates the stylopharyngeus muscle, which is involved in swallowing. Improper development of this nerve could affect the ability to swallow food and suckle. None of the pups found dead on the first day after birth had milk in their stomachs. Many were also cyanotic, indicating a difficulty in breathing, which may also indicate defects in the formation of the Xth nerve. The function of the Xth nerve could be affected by misrouting of signals which would normally be connected through the IXth nerve. Interestingly, a small number of $Hoxb3^{-/-}$ newborns were also found dead soon after birth, consistent with the low frequency of the IXth cranial nerve defects seen in the *Hoxb3* mutant embryos.

The full range of functions mediated by group 3 paralogous genes should become evident from the analysis of the triple mutants. This analysis, however, is technically hampered because most mice heterozygous for all three group 3 genes die before weaning. The death of the triple heterozygotes is surprising since mice heterozygous for the individual genes appear normal, are fertile, and live normal life spans. In addition, most *Hoxb3* mutant homozygotes also appear normal and are fertile. The observed death of the triple heterozygotes again stresses the importance of the quantitative balance of regional *Hox* gene expression during embryonic development.

In summary, through the analysis of the *Hox* group 3 double mutants, we have demonstrated that all three paralogous genes interact to form multiple structures within the throat region of the embryo. This includes tissues of separate embryonic regions. The nature of the interactions suggests that the individual functions of these *Hox* genes during development are of less importance than the summation of their activities. In a number of contexts the different paralogous genes appear to be performing equivalent functions.

ACKNOWLEDGMENTS

We thank C. Lenz, M. Allen, G. Peterson, E. Nakashima, M. Wagstaff, and S. Barnett for excellent technical assistance and L. Oswald for preparation of the manuscript. The 2H3 neurofilament hybridoma was obtained from the Developmental Studies Hybridoma Bank under Contract N01-HD-6-2915 from the NICHD.

REFERENCES

Barrow, J. R., and Capecchi, M. R. (1996). Targeted disruption of the *hoxb-2* locus in mice interferes with expression of *hoxb-1* and *hoxb-4*. *Development* **122,** 3817–3828.

Boulet, A. M., and Capecchi, M. R. (1996). Targeted disruption of *hoxc-4* causes esophageal defects and vertebral transformations. *Dev. Biol.* **177,** 232–249.

Capecchi, M. R. (1997). The role of *Hox* genes in hindbrain development. *In* "Molecular and Cellular Aspects of Neural Development" (W. M. Cowan, T. M. Jessell, and S. L. Zipursky, Eds.). Oxford Univ. Press, New York.

Chen, F., and Capecchi, M. R. (1997). Targeted mutations in *Hoxa-9* and *Hoxb-9* reveal synergistic interactions. *Dev. Biol.* **181,** 186–196.

Chisaka, O., and Capecchi, M. R. (1991). Regionally restricted developmental defects resulting from targeted disruption of the mouse homeobox gene *hox-1.5*. *Nature* **350,** 473–479.

Chisaka, O., Musci, T. S., and Capecchi, M. R. (1992). Developmental defects of the ear, cranial nerves and hindbrain resulting from targeted disruption of the mouse homeobox gene *hox-1.6*. *Nature* **355,** 516–520.

Condie, B. G., and Capecchi, M. R. (1993). Mice homozygous for a targeted disruption of *Hoxd-3* (*Hox-4.1*) exhibit anterior transformations of the first and second cervical vertebrae, the atlas and the axis. *Development* **119,** 579–595.

Condie, B. G., and Capecchi, M. R. (1994). Mice with targeted disruptions in the paralogous genes *hoxa-3* and *hoxd-3* reveal synergistic interactions. *Nature* **370,** 304–307.

Davis, A. P., and Capecchi, M. R. (1994). Axial homeosis and appendicular skeleton defects in mice with a targeted disruption of *hoxd-11*. *Development* **120,** 2187–2198.

Davis, A. P., and Capecchi, M. R. (1996). A mutational analysis of the 5′ Hox D genes: Dissection of genetic interactions during limb development in the mouse. *Development* **122,** 1175–1185.

Davis, A. P., Witte, D. P., Hsieh-Li, H. M., Potter, S. S., and Capecchi, M. R. (1995). Absence of radius and ulna in mice lacking *hoxa-11* and *hoxd-11*. *Nature* **375,** 791–795.

Davis, C. A., Holmyard, D. P., Millen, K. J., and Joyner, A. L. (1991). Examining pattern formation in mouse, chicken and frog embryos with an *En*-specific antiserum. *Development* **111,** 287–298.

Dodd, J., Morton, S. B., Karagogeos, D., Yamamoto, M., and Jessell, T. M. (1988). Spatial regulation of axonal glycoprotein expression on subsets of embryonic spinal neurons. *Neuron* **1,** 105–116.

Dollé, P., Dierich, A., LeMeur, M., Schimmang, T., Schuhbaur, B., Chambon, P., and Duboule, D. (1993). Disruption of the *Hoxd-13* gene induces localized heterochrony leading to mice with neotenic limbs. *Cell* **75,** 431–441.

Duboule, D. (1994). Temporal colinearity and the phylotypic progression: A basis for the stability of a vertebrate Bauplan and the evolution of morphologies through heterochrony. *Development* **(Suppl.),** 135–142.

Duboule, D., and Dollé, P. (1989). The structural and functional organization of the murine *Hox* gene family resembles that of *Drosophila* homeotic genes. *EMBO J.* **8,** 1497–1505.

Favier, B., Rijli, F. M., Fromental-Ramain, C., Fraulob, V., Chambon, P., and Dollé, P. (1996). Functional cooperation between the non-paralogous genes *Hoxa-10* and *Hoxd-11* in the developing forelimb and axial skeleton. *Development* **122,** 449–460.

Fromental-Ramain, C., Warot, X., Lakkaraju, S., Favier, B., Haack, H., Birling, C., Dierich, A., Dollé, P., and Chambon, P. (1996). Specific and redundant functions of the paralogous *Hoxa-9* and *Hoxd-9* genes in forelimb and axial skeleton patterning. *Development* **122,** 461–472.

Gendron-Maguire, M., Mallo, M., Zhang, M., and Gridley, T. (1993).

Hoxa-2 mutant mice exhibit homeotic transformation of skeletal elements derived from cranial neural crest. *Cell* **75,** 1317–1331.

Goddard, J. M., Rossel, M., Manley, N. R., and Capecchi, M. R. (1996). Mice with targeted disruption of *Hoxb-1* fail to form the motor nucleus of the VIIth nerve. *Development* **122,** 3217–3228.

Graham, A., Papalopulu, N., and Krumlauf, R. (1989). The murine and *Drosophila* homeobox gene complexes have common features of organization and expression. *Cell* **57,** 367–378.

Graham, A., Papalopulu, N., Lorimer, J., McVey, J. H., Tuddenham, E. G. D., and Krumlauf, R. (1988). Characterization of a murine homeo box gene, *Hox-2.6,* related to the *Drosophila Deformed* gene. *Genes Dev.* **2,** 1424–1438.

Hérault, Y., Hraba-Renevey, S., van der Hoeven, F., and Duboule, D. (1996). Function of the *Evx-2* gene in the morphogenesis of vertebrate limbs. *EMBO J.* **15,** 6727–6738.

Holland, P. W. H., and Garcia-Fernandez, J. (1996). *Hox* genes and chordate evolution. *Dev. Biol.* **173,** 382–395.

Horan, G. S. B., Kovàcs, E. N., Behringer, R. R., and Featherstone, M. S. (1995a). Mutations in paralogous *Hox* genes result in overlapping homeotic transformations of the axial skeleton: Evidence for unique and redundant function. *Dev. Biol.* **169,** 359–372.

Horan, G. S. B., Ramírez-Solis, R., Featherstone, M. S., Wolgemuth, D. J., Bradley, A., and Behringer, R. R. (1995b). Compound mutants for the paralogous *hoxa-4, hoxb-4,* and *hoxd-4* genes show more complete homeotic transformations and a dose-dependent increase in the number of vertebrae transformed. *Genes Dev.* **9,** 1667–1677.

Jeannotte, L., Lemieux, M., Charron, J., Poirier, F., and Robertson, E. J. (1993). Specification of axial identity in the mouse: Role of the *Hoxa-5* (*Hox-1.3*) gene. *Genes Dev.* **7,** 2085–2096.

Kostic, D., and Capecchi, M. R. (1994). Targeted disruptions of the murine *hoxa-4* and *hoxa-6* genes result in homeotic transformations of components of the vertebral column. *Mech. Dev.* **46,** 231–247.

Lee, K.-F., Li, E., Huber, L. J., Landis, S. C., Sharpe, A. H., Chao, M. V., and Jaenisch, R. (1992). Targeted mutation of the gene encoding the low affinity NGF receptor p75 leads to deficits in the peripheral sensory nervous system. *Cell* **69,** 737–749.

LeMouellic, H., Lallemand, Y., and Brûlet, P. (1992). Homeosis in the mouse induced by a null mutation in the *Hox-3.1* gene. *Cell* **69,** 251–264.

Lufkin, T., Dierich, A., LeMeur, M., Mark, M., and Chambon, P. (1991). Disruption of the *Hox-1.6* homeobox gene results in defects in a region corresponding to its rostral domain of expression. *Cell* **66,** 1105–1119.

Manley, N. R., and Capecchi, M. R. (1995). The role of *hoxa-3* in mouse thymus and thyroid development. *Development* **121,** 1989–2003.

Mansour, S. L., Thomas, K. R., and Capecchi, M. R. (1988). Disruption of the proto-oncogene *int-2* in mouse embryo-derived stem cells: A general strategy for targeting mutations to non-selectable genes. *Nature* **336,** 348–352.

Ramirez-Solis, R., Zheng, H., Whiting, J., Krumlauf, R., and Bradley, A. (1993). *Hoxb-4* (*Hox-2.6*) mutant mice show homeotic transformation of a cervical vertebra and defects in the closure of the sternal rudiments. *Cell* **73,** 279–294.

Rancourt, D. E., Tsuzuki, T., and Capecchi, M. R. (1995). Genetic interaction between *hoxb-5* and *hoxb-6* is revealed by nonallelic noncomplementation. *Genes Dev.* **9,** 108–122.

Rijli, F. M., Mark, M., Lakkaraju, S., Dierich, A., Dollé, P., and Chambon, P. (1993). A homeotic transformation is generated in the rostral branchial region of the head by disruption of *Hoxa-2,* which acts as a selector gene. *Cell* **75,** 1333–1349.

Satokata, I., Benson, G., and Maas, R. (1995). Sexually dimorphic sterility phenotypes in *Hoxa10*-deficient mice. *Nature* **374,** 460–463.

Sham, M. H., Hunt, P., Nonchev, S., Papalopulu, N., Graham, A., Boncinelli, E., and Krumlauf, R. (1992). Analysis of the murine *Hox-2.7* gene: Conserved alternative transcripts with differential distributions in the nervous system and the potential for shared regulatory regions. *EMBO J.* **11,** 1825–1836.

Small, K. M., and Potter, S. S. (1993). Homeotic transformations and limb defects in *HoxA-11* mutant mice. *Genes Dev.* **7,** 2318–2328.

Studer, M., Lumsden, A., Ariza-McNaughton, L., Bradley, A., and Krumlauf, R. (1996). Altered segmental identity and abnormal migration of motor neurons in mice lacking *Hoxb-1. Nature* **384,** 630–634.

Suemori, W., Takahashi, N., and Noguchi, S. (1995). *Hoxc-9* mutant mice show anterior transformation of the vertebrae and malformation of the sternum and ribs. *Mech. Dev.* **51,** 265–273.

Thomas, K. R., and Capecchi, M. R. (1987). Site-directed mutagenesis by gene targeting in mouse embryo-derived stem cells. *Cell* **51,** 503–512.

Zákány, J., and Duboule, D. (1996). Synpolydactyly in mice with a targeted deficiency in the *HoxD* complex. *Nature* **384,** 69–71.

Received for publication July 24, 1997
Accepted September 17, 1997